FIBRES & TEXTILES in Eastern Europe

sciendo

FIBRES & TEXTILES in Eastern Europe

Research Article • DOI: 10.2478/ftee-2023-0005 FTEE • 31(1) • 2023 • 38–51

# Study on Low-Velocity Impact Behavior of Twaron® Fabric Subjected to Double-Impactor Impact from a Numerical Analysis Perspective

Canyi Huang[1], Lina Cui[1], Yiping Qiu[1], Yajun Liu[2S*]

[1] College of Textiles and Apparel, Quanzhou Normal University, Quanzhou 362000, China
[2] Faculty of Textile Science and Technology, Shinshu University, 3-15-1 Tokida, Ueda 386-8567, Japan
* Corresponding author. E-mail: liuyajun1990@gmail.com

**Abstract**
In the present study, a finite element impact model was developed and analyzed using commercial FEM code ANSYS® and then validated via a drop-weight impact experiment. Moreover, double-impactor impact models were designed and developed with different impact distribution and locations of two impactors to compare impact properties. A total of 18 impact scenarios comprised of asymmetric and symmetric types were performed. The effect of impact location on the impact resistance force and duration time was investigated: the closer the impact point is to the fabric center, the longer the impact duration time. In addition, the effect of impact location on impactor failure deflection was also investigated and it was concluded that regardless of the symmetric or asymmetric impact scenario, the smaller the average distance between the impact location of the two impactors from the fixed boundary, the smaller the overall average failure deflection that occurs. The relevance of impact location and fabric energy absorption capacity was also identified. Furthermore, the effect of impact location on fabric stress distribution and transverse deformation and of the variation of the impact velocity on fabric impact behaviors were investigated. These findings will provide important guidance for engineering soft body armor and composite materials.

**Keywords**
Double-impactor; low-velocity; impact behavior; numerical analysis.

## 1. Introduction

Selected fabrics comprise of high strength and high stiffness para-aramid continuous-filament materials, including Twaron® (Teijin), Kevlar® (DuPont), PBO fibers such as Zylon® (Toyobo), and ultra-heavy molecular weight polyethylene (UHMWPE) such as Spectra® (Allied Signal), commonly used in military body armor to provide ballistic and blast protection, leading to better performance and lighter weight of body armor [1]. In addition, fabrics as composite materials are used to provide protective layers for aircraft engine cowlings against fragments during service, marine structure hulls against underwater blast impulse, and vehicles operating in landmine-risk areas.[2]

Several studies have been performed to explore the impact behavior of these high-performance fabrics. [3-8] The investigation methods for the impact behavior of these high-performance fabrics have been confined to empirical, analytical and numerical methods. The empirical method uses experimental data to investigate ballistic impact responses and different mechanisms in material failure. This method may be the most straightforward, but it is expensive and time consuming.

The analytical method uses governing equations based on general mechanical laws to analyze various parameters involved in the ballistic impact process. In the analytic process of a ballistic impact, the whole process is divided into certain steps by a small increment of time, then step by step until the designated ultimate time; all the equations at every time increment are derived. When comparing the analytic method with the empirical method, the analytical method consumes less or no materials and uses less labor. However, it requires a complete understanding of the ballistic impact process.

The numerical method uses finite element (FE), theory, and commercial computer software (such as Abaqus, ANSYS, and LS-DYNA) to establish a projectile-fabric simulation model for elucidating the mechanism behind a fabric subjected to impact. This method is frequently preferred and implemented by researchers. Several researchers used the [9-15] numerical method to determine the effect of physical, energy absorption, failure modes, weave type, and yarn mechanical properties, as well as the influence of ply orientation on the penetration mechanism of fabrics. In addition, the use of numerical modeling methods to determine the boundary conditions has proven effective.

Virtual testing through computational simulation has gained increasing interest over the past decade, and is receiving growing attention as an instrument to explore new materials, structures, and boundary conditions efficiently through parametric studies. This method is also used for the analysis and identification of various mechanisms of deformation, fracture, and energy dissipation which cannot be simply acquired through experimental methods. Owing to computing technology developments, the impact behavior of high-performance fabrics is hierarchically characterized into three length scales, such as micro-scale for fibers (~$10^{-3}$ mm), meso-scale for yarns (~$10^{-1}$ mm), and macro-scale for fabrics (~$10^{2}$ mm). These different scales

can be deeply studied using numerical tools [16].

Due to the complication and high computational cost of the numerical method, only a few mechanical studies of fabrics have been conducted at a micro-scale (i.e., on fibers) [17-18]. In macro-scale modeling, homogeneous material properties of a fabric sheet are considered, and membrane elements are frequently modeled [19–21]. Macro-scale modeling is the most computationally efficient among the three modeling techniques. However, yarn sliding and yarn pullouts of fabric under external loading cannot be simulated in macro-scale models; hence, the actual reaction behavior of fabrics under impacts cannot be well performed. While at a meso-scale, yarns are considered a homogeneous continuum, which are modeled using either shell elements or a hexahedron. Modeling fabrics at the yarn level allowed the capturing of interactions between yarns as well as between the projectile and yarns. Work on modeling fabrics at a meso-scale is relatively more extensive in literature than for the other two scales [22–30]. Therefore, this study used the numerical meso-scale modeling method to investigate the impact response of high-performance fabric.

In summary, several studies have been carried out on the impact behavior of high-performance fabric using different methods and tools. However, most existing studies focused on the single-impactor-based impact scenario of soft body armor. Studies on double-impactor-based scenarios are limited due to more complexity and computational cost. Nevertheless, deeper study on the impact behavior of soft body armor under a multiple-impactor impact is beneficial for enhancing body armor power. Therefore, it is urgent for engineers to develop high-performance fabrics with all-around improved performance in impact resistance.

The present numerical study focuses on the impact performance of Twaron® fabric using meso-scale modeling in ANSYS®. The impact performance and failure mechanism of high-performance fabrics under a double-impactor impact were investigated. The influence of the distribution and location, as well as the change of impact velocity of two impactors on the impact behavior of Twaron® fabric were also investigated.

## 2. Experimental and numerical framework

### 2.1. Experimental setup

The drop-weight test program was performed using a 9250HV INSTRON™ Pneumatic Dynatup test system. A schematic diagram of the impact tester is shown in Fig. 1. The impactor, made from high rigid 4340 steel, has a hemispherical head of 12.7 mm standard diameter. During the impact test, the hemisphere-head-impactor was dropped from a predetermined height, which then hit the center of the test sample in between the round-clamped plates. An anti-rebound system was attached to the testing machine to prevent multiple impacts on the same specimen. The specimens were supported on a pair of pneumatically clamped rings having an internal diameter of 40 mm. The low-velocity impact tests were performed according to the ASTM standard (D7316). A minimum impact weight of about 7 kg was used for all the tests. Two impact loading and acceleration sensors were attached to the impactor. Sensors were used to measure the contact force between the impactor and specimen and the acceleration during the low-velocity impact. Based on the impact loading $F$(t) test, calculation of the acceleration α(t), initial velocity $vi$, velocity $v$(t), and displacement $D$(t) of the impactor and the absorbed energy $E$(t) of the specimen was possible according to equations 1-3[31]

$$v(t) = vi + \int_0^T \alpha(t)\,dt \qquad (1)$$

$$D(t) = \int_0^T v(t)dt \qquad (2)$$

$$E(t) = \int_0^T F(t)v(t)dt \qquad (3)$$

Light weight and high strength plain-woven Twaron® CT 612, made by

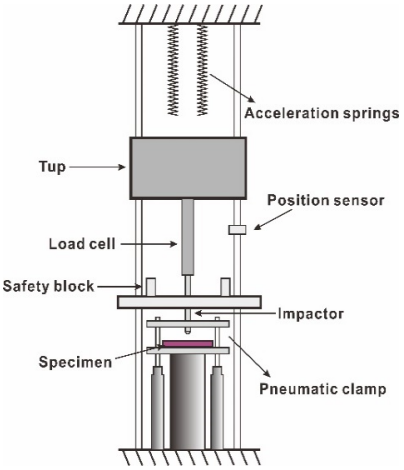


*Fig. 1. Schematics of impact tester 9250HV*

TEIJIN®, was used in this study. This fabric was manufactured using a plain weave of 110×110 yarns (per mm$^2$), each of which consisting of 500 filaments. The bulk and linear density were 1440 kg/m$^3$ and 550 dtex. 5 mm thickness plywood plates cut to 100 mm × 100 mm with a 70 mm diameter hole cut in the middle were used to sandwich and glue a fabric sample of 100 mm × 100 mm size. This effective specimen design method solves the problem that the fabric is too soft and cannot be fixed firmly. Front and side views of the specimen after impact at 10 m/s are shown in Fig. 2.

### 2.2. Low-velocity impact simulation

A commercial explicit nonlinear FEA code (ANSYS®-AUTODYN) was employed for FE modeling of a low-velocity drop weight impact on a Twaron® fabric. The fabric model was simulated at yarn level (meso-scale). The cross-section of the yarn was modeled as a lenticular shape, assumed as a continuous solid with the same properties as fibers. The height, width, and wavelength of the yarn cross-section were set as 0.1, 0.9, and 1.8mm, respectively, according to measurements of the real fabric by a digital microscope, from which the geometrical fabric model was deduced. The fabric model was created to be circular in shape with a diameter of 70 mm by considering the nature of clamping applied in the tests. The boundary condition of a complete

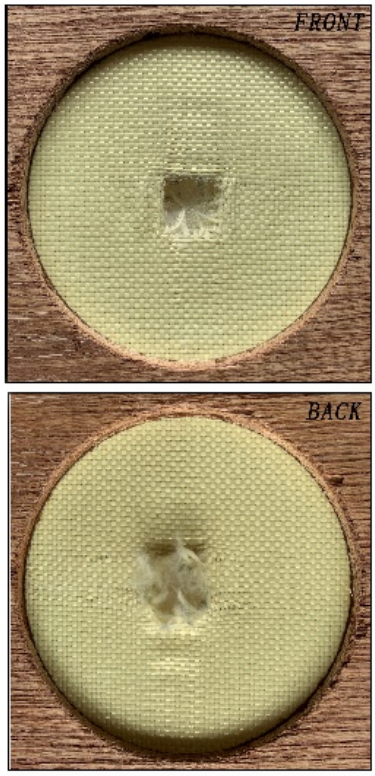


*Fig. 2. Both specimen sides after impact at 10m/s*

fix around the fabric circumference was adopted. And a hemisphere-head-impactor with a diameter of 12.7 mm was simulated.

In addition, transversely isotropic material properties were applied to the yarn model, which were combined to create a fabric model. The material constants for the transversely isotropic aramid yarn were dominated by the longitudinal tensile modulus ($E_{11}$), and the transverse elastic moduli ($E_{22}$ and $E_{33}$) and shear moduli ($G_{12}$, $G_{13,}$ and $G_{23}$) were assumed to be smaller than $E_{11}$, while the Poisson's ratios were set as $v_{12} = v_{13} = v_{23} = 0$. Although the Poisson's ratio of the real material cannot be 0, considering that the real yarn is composed of countless fiber materials, the value of Poisson's ratio of the yarn in simulation is determined by the characteristics of fiber movement inside the yarn. The material constants used in the FE modeling were: $E_{11} = 72.63$ GPa, $E_{22} = E_{33} = 1.13$ GPa and $G_{12} = G_{13} = G_{23} = 1.04$ GPa. Furthermore, a friction coefficient of 0.3 was designated to yarn/yarn contact, which was obtained from experiments in our previous study [32], while the friction coefficient between the impactor and yarns was designated as 0.2 [33]. Mesh sensitivity studies were carried out and results suggested that 167,860 eight-node solid brick elements meshed in the impact model were reasonable for the low-velocity impact simulation. The criterion of maximum principal strain failure determined as element erosion was considered: that is when $\varepsilon \geq \varepsilon_f$, the element failed and was taken away from the model calculation, where $\varepsilon_f$ demonstrated the yarn's failure strain, set as 3.9%.

## 2.3. Model validation

On the basis of the aforementioned experimental setup, impact tests of Twaron® fabric were performed at velocities between 8-16 m/s with a 2 m/s interval. At least six samples were impacted repeatedly at every designated velocity for reproducibility. From Fig. 2, it can be seen that the circular boundary of the fabric was well fixed by the plywood plates, and significant damage appeared in the fabric's primary yarns (primary yarns in this paper refer to two groups of crossover yarns that pass through the center of the fabric, which directly contact with the impactor). Simultaneously, simulations with the same impact velocities were also performed. Correlation of simulation prediction results and mean experiment results are shown in Figure 3(a) and (b), where the gradients of the regression line are 0.9963 and 0.9988, which validate the model accuracy. In addition, Figure 3(c) demonstrates a comparison of results of the F-T curve between the experiment and simulation at an impact velocity of 10m/s and 16m/s, respectively. Approximate curves at the same impact velocity also verify the validity and success of the impact model created in this study.

## 2.4. Simulation of fabric subjected to double-impactor-impact

Two impactors of the same type were applied to simulate the simultaneous impact of the fabric and to effectively analyze the effect of location on the impact response of the fabric. The impactors were designed with half of the diameter and mass of the real impactor. The impact model is shown in Fig.4. The impact center positions on the fabric in different impact scenarios are shown in Fig.5. The impact locations: O, A, B, C, $A_1$, $B_1$, and $C_1$ were in the center of primary yarns. These points divide the central primary yarn into eight equal parts. Summarily, impact locations D, $D_1$, E, $E_1$, F, and $F_1$ were on a line 45° to the above central primary yarn, and impact locations $D_2$, $E_2$, and $F_2$ are on a line 45° to the above central primary yarn.

For instance, impact scenario $IAA_1$ indicates the impact event when the impact of the two impactors are in positions A and A1. Different types of 18 impact models were developed. 18 simulations of impact scenarios were performed according to IOA, IOB, IOC, IOD, IOE, and IOF, which are asymmetrical impacts with one impactor impacting the fabric center. and IAB, IAC, and IBC, which are asymmetrical impacts without an impactor impacting the fabric center. While scenarios $IAA_1$, $IBB_1$, $ICC_1$, $IDD_1$, $IEE_1$, $IFF_1$, $IDD_2$, $IEE_2$, and $IFF_2$ are symmetrical impacts without an impactor impacting the fabric center. Generally, an average calculation time of 64 h was the cost of a scenario using a computer with an Intel xeon® 12 core CPU and 64G RAM configuration.

## 3. Results and discussion

### 3.1. Influence of impact location on impact resistance force and duration time

The resistance force is the reaction force applied by the fabric to the impactor, which is also a key index to judge the material's impact resistance ability. In this study, the yarns reached their fracture limit and started to break when the maximum resistance force of each impactor was reached at a particular impact duration time. The *F-T* history curve was plotted to compare the influence of impact location. The impactors that impacted positions O and N were named "impactor O and impactor N," respectively. The value

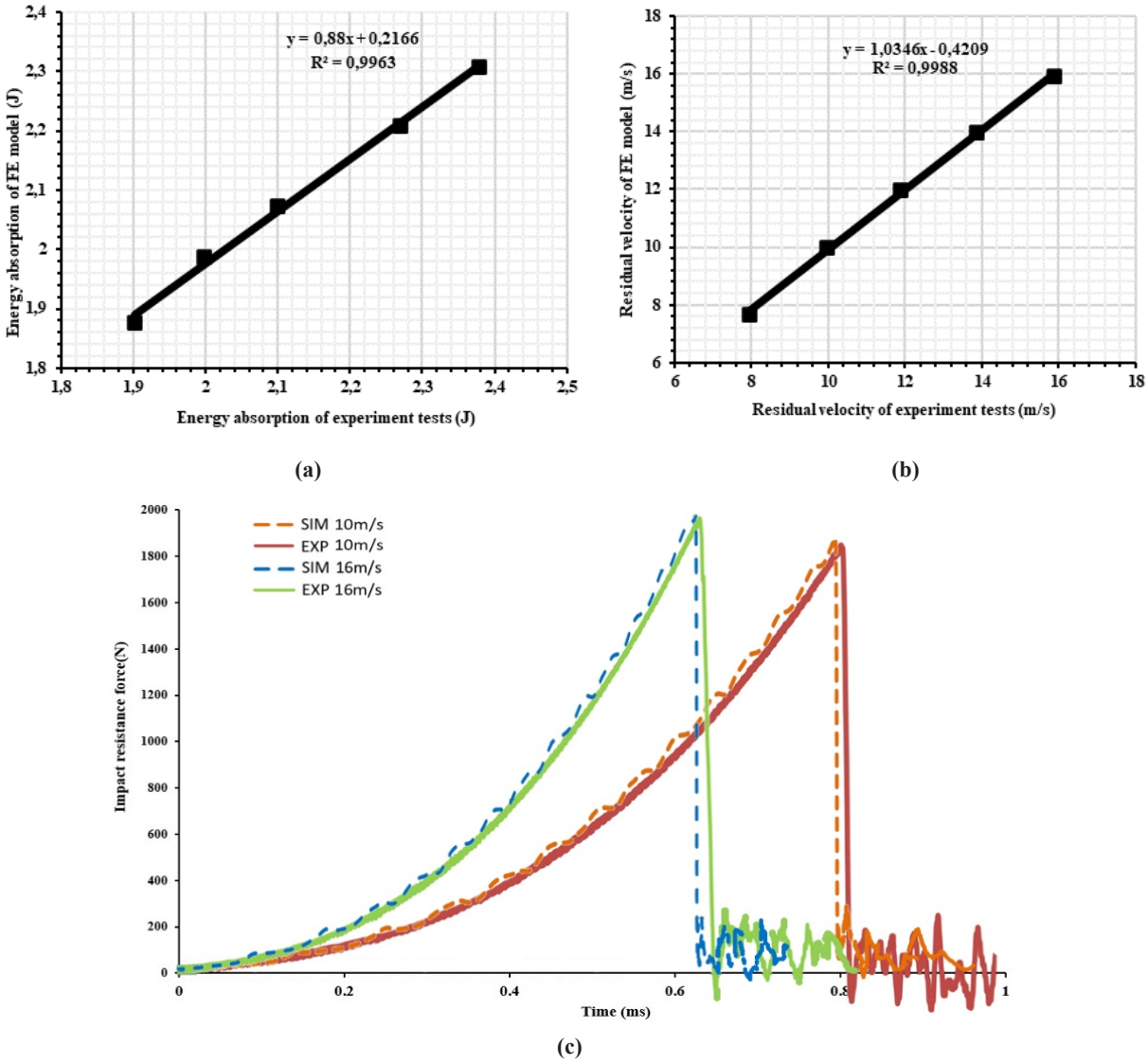


*Fig. 3. Comparison of simulation and experiment results: (a) energy absorption, (b) residual velocity, (c) F-T curve*

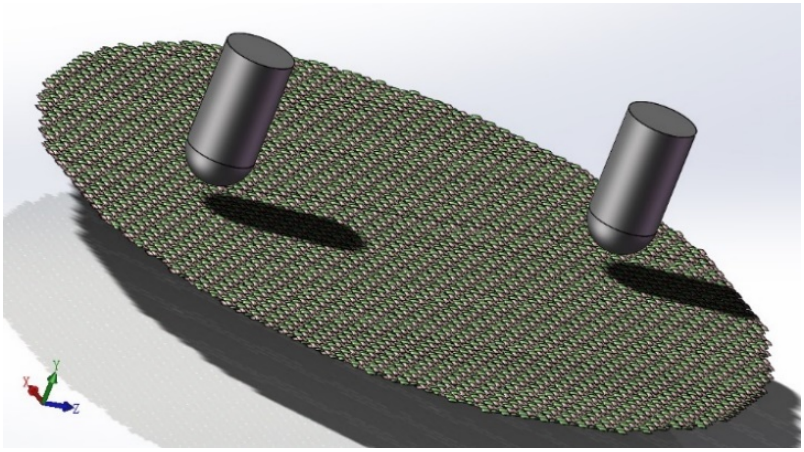

*Fig. 4. Impact model*

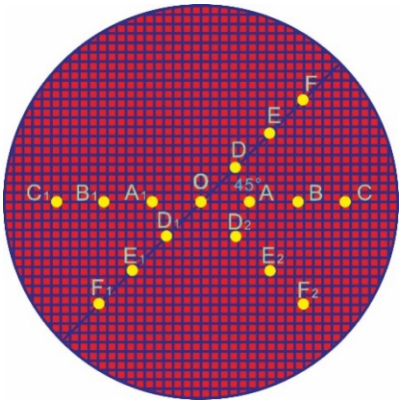


*Fig. 5. Schematic of impact center locations*

range of N = A, B, C, D, E, F, $A_1$, $B_1$, $C_1$, $D_1$, $E_1$, $F_1$, $D_2$, $E_2$, and $F_2$. For example, in the impact scenario IOA, impact N = impactor A, representing impactor impacted position A.

### *3.1.1. Asymmetrical impact scenarios*

Figures 6a−6c show the *F-T* curve of various asymmetrical impact scenarios. Figure 6a compares impact resistance forces of impactor O in double-impactor impact scenarios with one impactor impacting the fabric center. Similar curves were observed as the impact resistance force increased to a certain level. A drastic fall was observed at this level at a certain impact duration time. However, the influence of the maximum resistance force on another impact point of the fabric, such as IOC and IOB impact scenarios, shows some volatility curves before reaching maximum resistance. Impactor O was subjected to a higher maximum impact resistance force when the other impact point was located at the line inclined at 45° to the primary yarn center, contrary to that when the impact point was located at the yarn's primary center.

The average maximum impact resistance force of impactor O appearing in impact scenarios IOD, IOE, and IOF is 611.3N, whereas in impact scenarios IOA, IOB, and IOC it is 457.7N, which is 74.9% of the former one. There was no significant difference in the impact duration times needed to complete fracture at the fabric impact center in all impact scenarios. In addition, among the related impact scenarios, impact scenario IOD had the longest impact duration time of 0.706 ms, while impact scenario IOE had the shortest - 0.639 ms.

Figure 6(b) compares impact resistance forces of impactor N in asymmetrical double-impactor impact scenarios with one impactor impacting the fabric center. The variation in impact location has a significant effect on the impact duration time (i.e., the closer the impact point is to the fabric fixed boundary, the shorter the impact-resisting time). This effect can be attributed to the continued yarn fracture extension rate. Moreover, as the distance between the impact location and the fixed boundary decreases, the yarn fracture extension rate also decreases, reducing the fracture time (impact duration time).

The maximum resistance force showed little difference among the impact scenarios when impactor N impacted the yarns at primary center; however, it showed a large difference among the impact scenarios when impactor N impacted at the line inclined at 45° to the yarn's primary center. And among the impact scenarios, IOD had the highest maximum impact resistance force of 650.7N, while the IOF had the lowest - about 442.3N, which is only 68.0% of the former.

Figure 6c compares the impact resistance forces of impactor N in asymmetrical double-impactor impact scenarios without the impactor impacting o the fabric center. The impact resistance force of IAB-A indicated that in impact scenario IAB, the resistance force was applied from the fabric to impactor A. Similarly, it can be seen from the figure that the closer the impact point is to the fabric fixed boundary, the shorter the impact duration time. And among all impact scenarios compared, impactor A in impact scenario IAC had the highest maximum impact resistance force of about 577.3N, while impactor B in impact scenario IBC had the lowest - about 334.1N, which is only 57.9% of the previous one.

### *3.1.2. Symmetrical impact scenarios*

Figure 7 shows the *F-T* curve of various symmetrical impact scenarios. Due to the symmetrical impact of the fabric model and the impact location, the simulated experimental results showed some similarity between the two impactor parameters, such as the resistance force and fracture time at the impact location of the fabric. As a result, only the data from one impactor were used for analysis in this study. The variation observed at the impact location significantly affected both the impact resistance force and impact duration time (i.e., the closer the impact point is to the fabric center, the longer the impact duration time).

The average maximum resistance force in impact scenarios $IAA_1$, $IDD_1$, and $IDD_2$ is 636.4N, while that in in scenarios $IBB_1$, $IEE_1$, and $IEE_2$ is 600.6N, and for $ICC_1$, $IFF_1$, and $IFF_2$ - 492.5N, which is only 94.4% and 77.4%, respectively, of the former one. Similarly, the average duration time in impact scenarios $IAA_1$, $IDD_1$, and $IDD_2$ is 0.669 ms, while that in scenarios $IBB_1$, $IEE_1$, and $IEE_2$ is 0.558ms, and for $ICC_1$, $IFF_1$, and $IFF_2$ - 0.411 ms, which is only 83.4% and 61.4% of the former one, respectively.

## 3.2. Influence of impact location on impactor's failure deflection and energy absorption

Failure deflection refers to the impactor deflection, which occurs at fabric failure; it is considered as one of the important indices to study the impact behavior of soft body armor. Failure deflection is proportional to fabric impact duration time. Figure 8a displays a comparison of results of the failure deflection in different asymmetrical impact scenarios, previously discussed in the above section. The short distance between the impact location and fixed boundary leads to premature yarn breakage, which results in a smaller failure deflection. Thus, in the impact scenarios with impact locations located close to a fixed boundary, the difference in failure deflection between the two impactors was significant, while in other impact scenarios, the difference was not significant. The shorter average distance between the impact location of the two impactors and the fixed boundary led to little average failure deflection (Fig.8 a).

Figure 8b shows a comparison of results of failure deflection in different symmetrical impact scenarios; the data results are taken only from a single part due to the symmetrical characteristics. The impact location plays an important role in the impactor's failure deflection. In all the different impact scenarios, the same distance of the impact location from

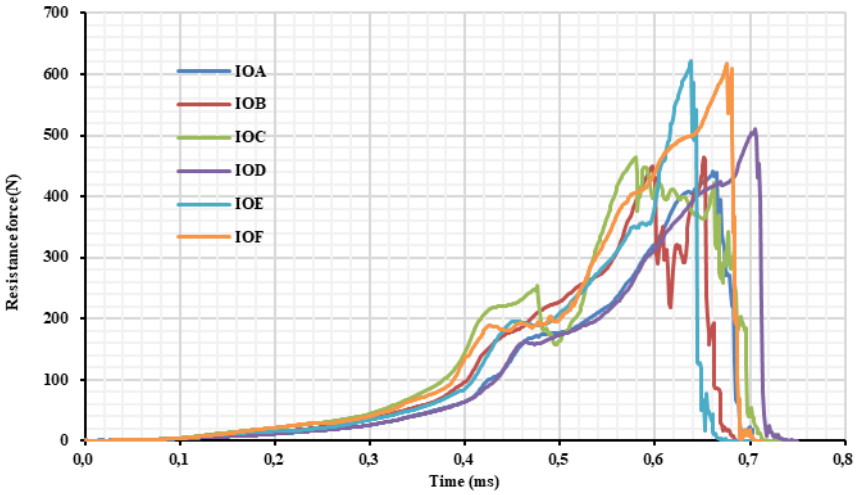


(a)

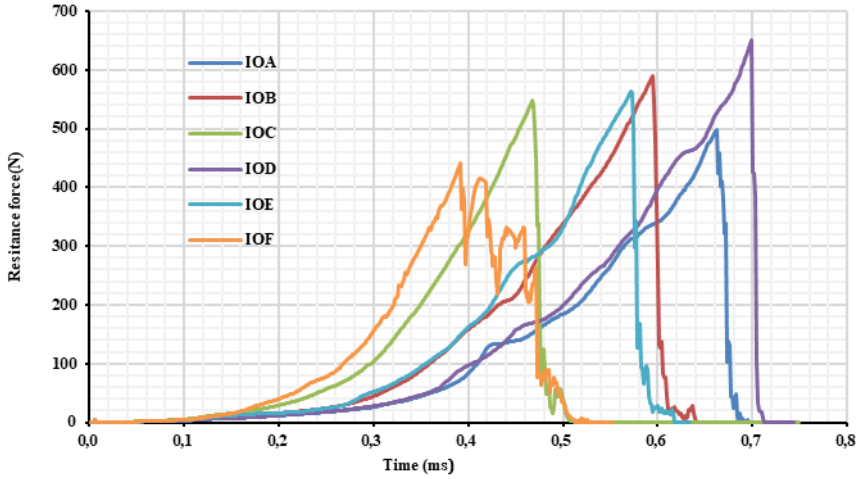


(b)

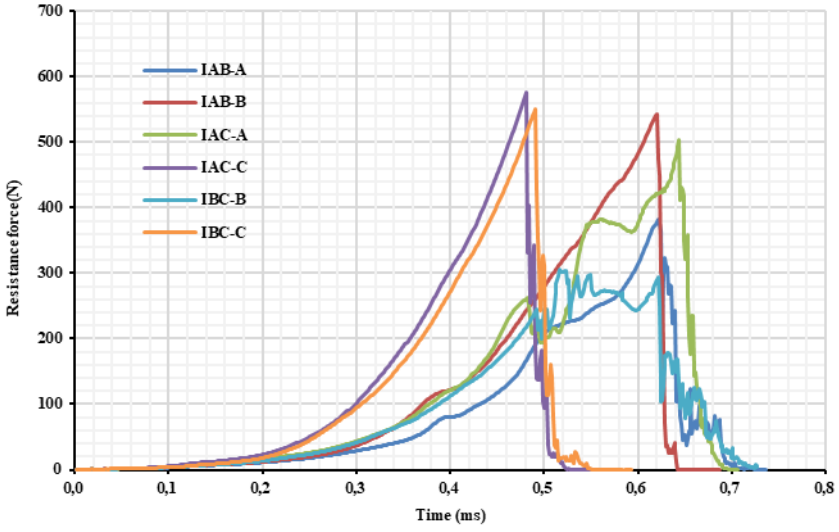


(c)

*Fig. 6. Comparison of resistance force history in different asymmetrical impact scenarios: (a) resistance force applied to impactor O, (b) resistance force applied to impactor N (with an impactor impacting the fabric center), (c) resistance force applied to impactor N (without impactor impacting the fabric center)*

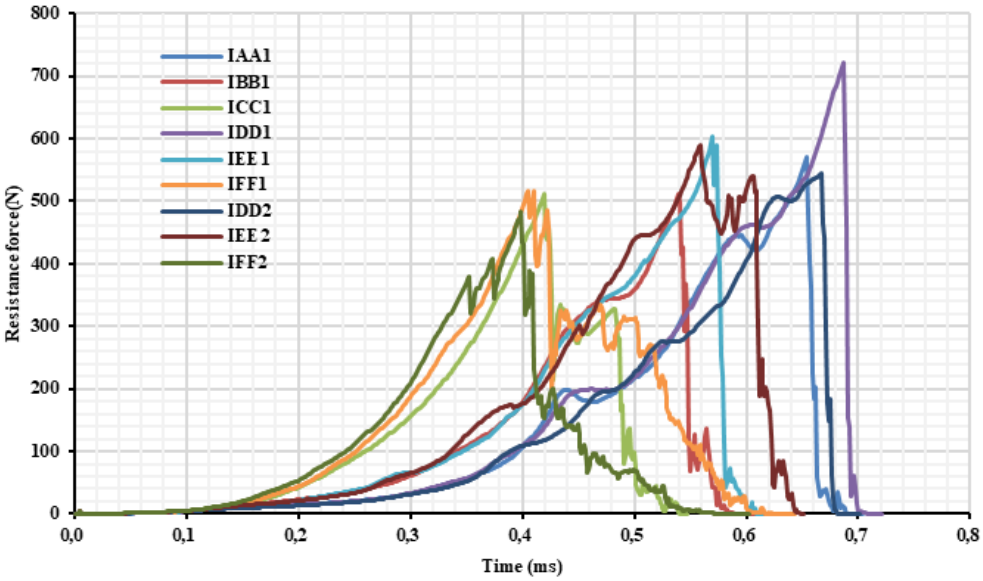


*Fig. 7. Comparison of resistance force history in different symmetrical impact scenarios*

the fabric center results in a similar failure deflection. Similar to the above findings, the smaller the average distance between the impact location of the two impactors from the fixed boundary, the smaller the overall average failure deflection that occurs.

Moreover, during the impact event, energy absorbed by the fabric was converted into strain energy and kinetic energies derived from the stretching and movement of the yarns. This energy was converted due to transverse deflection of the fabric and inward movement of yarn material towards the impact location. Hence, some of the energies absorbed by the fabric originated from the kinetic energy loss of the impactors. Thus, the total energy absorption of fabric E can be expressed by Equation 4.

$$E = \frac{1}{2}\left[M_1\left(V1_0{}^2 - V1_R{}^2\right) + + M_2\left(V2_0{}^2 - V2_R{}^2\right)\right] \quad (4)$$

where $M_1$ and $M_2$ are the masses of the impactors, $V1_0$ and $V2_0$ - the initial impact velocities, and $V1_R$ and $V2_R$ are the residual impact velocities of the two impactors, respectively.

Figure 9 displays the energy cost of the impactors and the total energy absorption

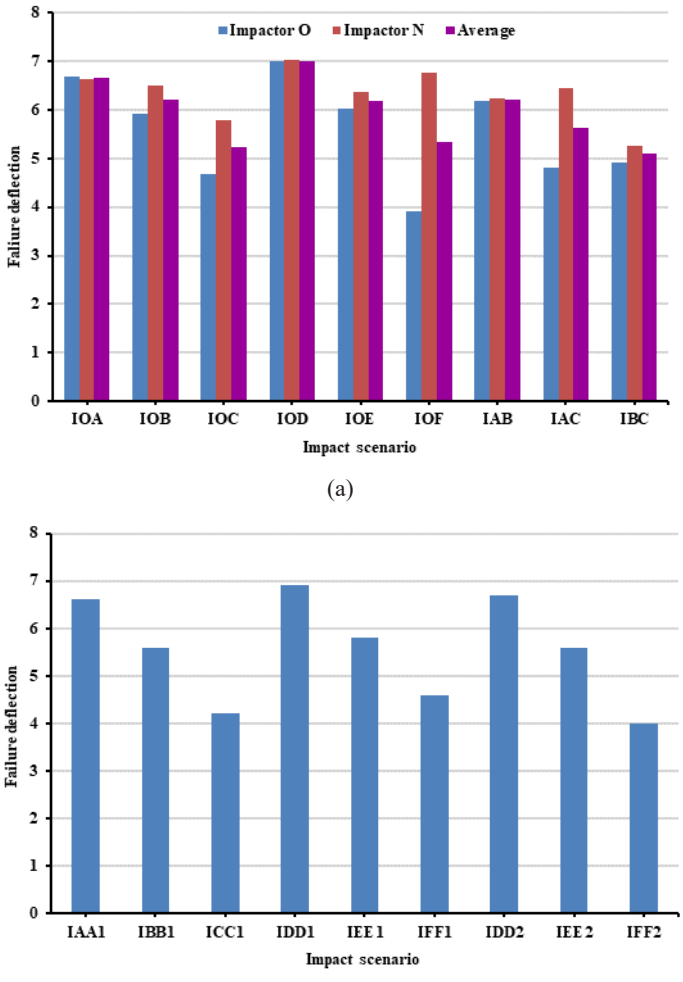


*Fig. 8. Comparison of failure deflection of impactors in different impact scenarios: (a) asymmetrical impact scenarios; (b) symmetrical impact scenarios*

of the fabric. Data of the asymmetrical impact scenarios are shown in Fig.9a. Impactor O exhibited the best energy absorption capacity in impact scenario IOF, while it exhibited the poorest in impact scenario IOA. Due to the earlier fracture of the yarn from the impactor closer to the fixed boundary, the energy absorption of the fabric (impactor C and F) became poorer. In the double-impactor impact asymmetrical scenarios, the greater the spacing of the impactors, the greater the difference in the energy absorption capacity of the fabric to impactor O and impactor N (Fig. 9a). Generally, among all asymmetrical impact scenarios, the fabric shows the best performance in scenario IOD with a total energy absorption of 1.93J, followed by scenario IOF with 1.70J, while the poorest performance appears in scenario IBC 1.34 J, which is only 69.4% of that in scenario IOD.

Data of symmetrical impact scenarios are plotted in Fig.9b. When comparing symmetrical impact scenarios to asymmetrical impact scenarios, the data from symmetrical impact scenarios appear to be more dispersed. Similar to the above findings, impact scenarios $ICC_1$, $IFF_1$, and $IFF_2$ of the impactors closer to the fixed boundary resulted in a poor energy absorption capacity of the fabric. The fabric performed best in impact scenario $IDD_1$ with a total energy absorption of 2.20J, which is also the best performance among all asymmetrical and symmetrical scenarios, followed by scenario $IAA_1$ with 1.88J, while the poorest performance appears in scenario IBC with 1.26J, which is also the poorest performance among all asymmetrical and symmetrical scenarios.

## 3.3. Influence of impact location on fabric stress distribution and transverse deformation

### *3.3.1. Asymmetrical impact scenarios*

Figure10 shows the variation in Von-Mises stress distribution contours of fabrics undergoing a double-impactor impact with different impact locations at different moments. In the initial stage of the impact, the overall stress was low due to the decrimp effect of yarns and subsequent spread to all primary yarns and then secondary yarns. Subsequently, the stressed areas generated by the two impactors started to overlap each other as the impact continued at a location closer to the fixed boundary. First, the yarns reached the maximum stress and then fractured, allowing the other impactors to penetrate the fabric faster.

A comparison of stress distribution contours in impact scenarios IOD, IOE, and IOF was made. In the asymmetrical impact scenarios with one impactor impact at the fabric center, impactor N moved farther from the center of the fabric. As a result of this movement, a larger maximum stress and wider stressed area were observed. In addition, a faster fracture of the fabric by impactor N was also clearly observed . From the comparison of results of asymmetrical impact scenarios IOC and IOF, with the same condition of one impactor impacting the fabric center as well as the same distance between the two impactors in the impact scenario, a larger fabric stress area caused by impactor O was found when impactor N was located in the center primary yarn.

However, a less stress area caused by impactor N was observed at the same impact moment before the first fabric fracture occurred when compared with the impact scenario with one impact location located 45° to the primary center yarn. Faster fracture of the fabric by impactor N was also observed in the former scenario. Generally, compared to the other scenarios, fabric in impact scenario IOD was more stressed before failure, leading to a longer impact duration time and better energy absorption capacity.

Figure 11 shows a comparison of fabric transverse deformation in asymmetrical impact scenarios. The fabric under impactor O is always harder to puncture than impactor N. The maximum transverse deformation caused by impactor N becomes smaller as the impact point moves further away from the center of the fabric regardless of the impact location at the primary yarn center. However, the maximum transverse deformation caused by impactor O has little difference among all impact scenarios.

### *3.3.2. Symmetrical impact scenarios*

Figure12 shows a comparison of the variation in Von-Mises stress distribution contours in impact scenarios $IAA_1$, $IBB_1$, $ICC_1$, $IDD_1$, $IEE_1$, and $IFF_1$. It was revealed that as impactor N moved farther from the fabric center in the asymmetrical impact scenarios without an impactor impact at the fabric center, a wider stressed area and larger maximum stress were observed under the same impact moment before the rapid fabric failure. The rapid fracture of the fabric led to inadequate stress of the fabric and resulted in less energy absorption with a poorer impact resistance capacity. In addition, in the impact scenarios with the impact location located at 45° to the primary center of yarn, the fabric is always more stressed in the same impact moment before failing (resulting in a better energy absorption capacity) than in the impact scenarios with the impact location located at the primary yarn center.

A comparison of fabric transverse deformation in symmetrical impact scenarios is shown in Fig.13. Similar to the asymmetrical impact scenarios, the maximum transverse deformation caused by impactors becomes smaller as the impact point moves further away from the center of the fabric, regardless of the arrangement of the impact location of the two impactors on the fabric. Impact scenario $IDD_1$ exhibited the largest maximum transverse deformation, while impact scenario $IFF_2$ exhibited the smallest. Therefore, impact scenario $IDD_1$ has the longest impact duration time, resulting in the best energy absorption capacity among all asymmetrical and symmetrical impact scenarios.

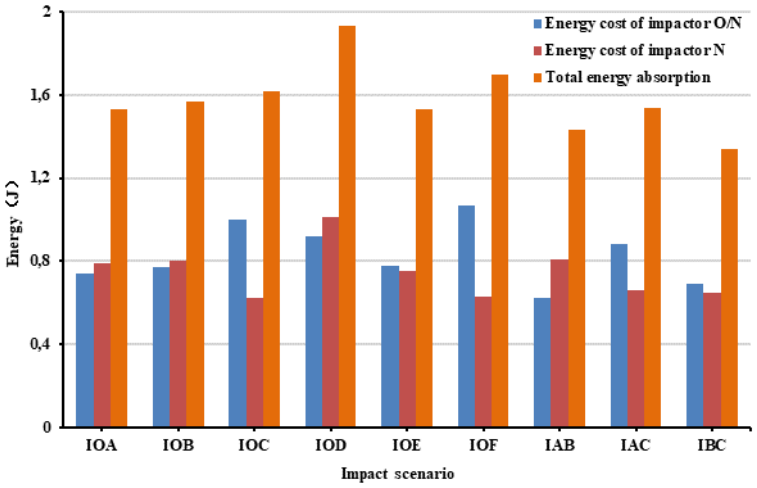


(a)

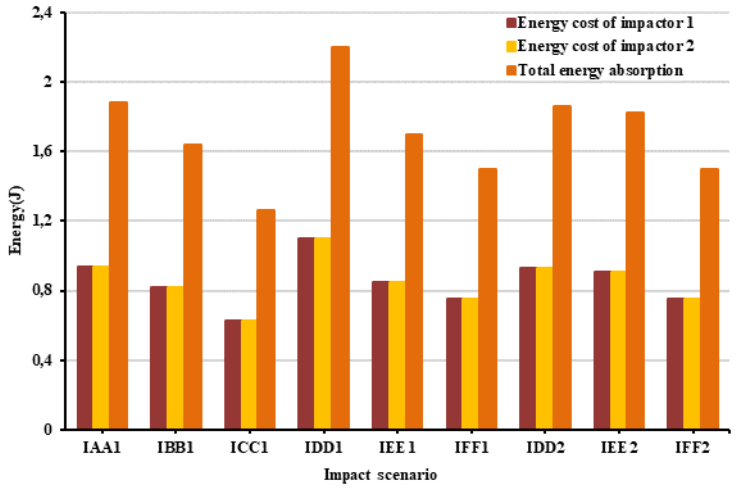


(b)

*Fig. 9. Energy cost of impactors and total energy absorption of fabric: (a) asymmetrical impact scenarios, (b) symmetrical impact scenarios*

## 3.4. Influence of variation in impact velocity on fabric impact behaviors

The influence of variation in the impact velocity on the behaviors of fabric were investigated, and impact scenarios $IDD_1$ and IOC were chosen as representative of symmetric and asymmetric impact scenarios, respectively. In symmetric impact scenario $IDD_1$, the velocity of one of the impactors ($V_1$=10m/s) was constant, while that of the other impactor ($V_2$) varied: 10 m/s, 9 m/s, 8 m/s, and 7 m/s. In asymmetric impact scenario IOC, the velocity of impactor O ($V_O$=10m/s) was constant, while the velocity of impactor C ($V_C$) varied: 10 m/s, 9 m/s, 8 m/s, and 7 m/s, resulting in the exchange of velocity between the two impactors. The impact results are listed table 1 and table 2. Parameters such as MF, T, and ET represent the maximum resistance force, impact endurance time, and total energy absorption, respectively.

In the symmetric impact scenario, the fabric's maximum resistance force and the fabric's impact endurance time for impactor 1 increase with a decreasing $V_2$ at a constant $V_1$; however, the fabric's maximum resistance force to impactor 2 and the total energy absorption decrease (Table 1). The constant $V_1$ of impactor 1 results in a slight increase in $MF_1$ and $T_1$, while the decreased velocity of impactor 2 results in a significant increase in $T_2$ but a significant decrease in $MF_2$. Generally, as the average impact velocity of impactors decreases, the energy absorption capacity of the fabric becomes weaker.

In the asymmetric impact scenario, $MF_O$, $T_O$, and $T_C$ increase with the decreasing velocity of impactor C (Vc) at a constant velocity of impactor O (Vo), while $MF_C$ decreases at the same conditions (Table 2). Conversely, $MF_C$ and $T_C$ initially decrease, then increase, and finally decrease with a decreasing Vo at a constant Vc, while $MF_O$ and $T_O$ decrease and increase, respectively. Generally, regardless of the change in velocity of either impactor, the lower the average impact velocity of impactors, the weaker the energy absorption capacity of the fabric.

## 4. Conclusions

Models of a double-impactor impact on Twaron® fabric were developed to investigate the effects of impact location and impact velocity on the impact behavior of high-performance fabric. The following findings were made:

- In the asymmetric impact scenario, impactor O was subjected to a higher maximum impact resistance force when the impact point was located along a line inclined at 45° to the primary center yarn; this was contrary to the impact point located at the primary center yarn. Moreover, fabric impact duration times for impactor O were relatively concentrated in all impact scenarios. The closer the impact point is to the fabric's fixed boundary, the shorter the fabric's impact duration time for impactor N. iImpact scenario IOD exhibited the largest maximum impact resistance force of 650.7N among all impact scenarios for impactor N.
- The closer the impact point is to the fabric center in the symmetric impact scenario, the longer the impact duration time. The average maximum resistance force increased as the impactor impact moved closer to the fabric center.
- Regardless of the symmetric or asymmetric impact scenario, the

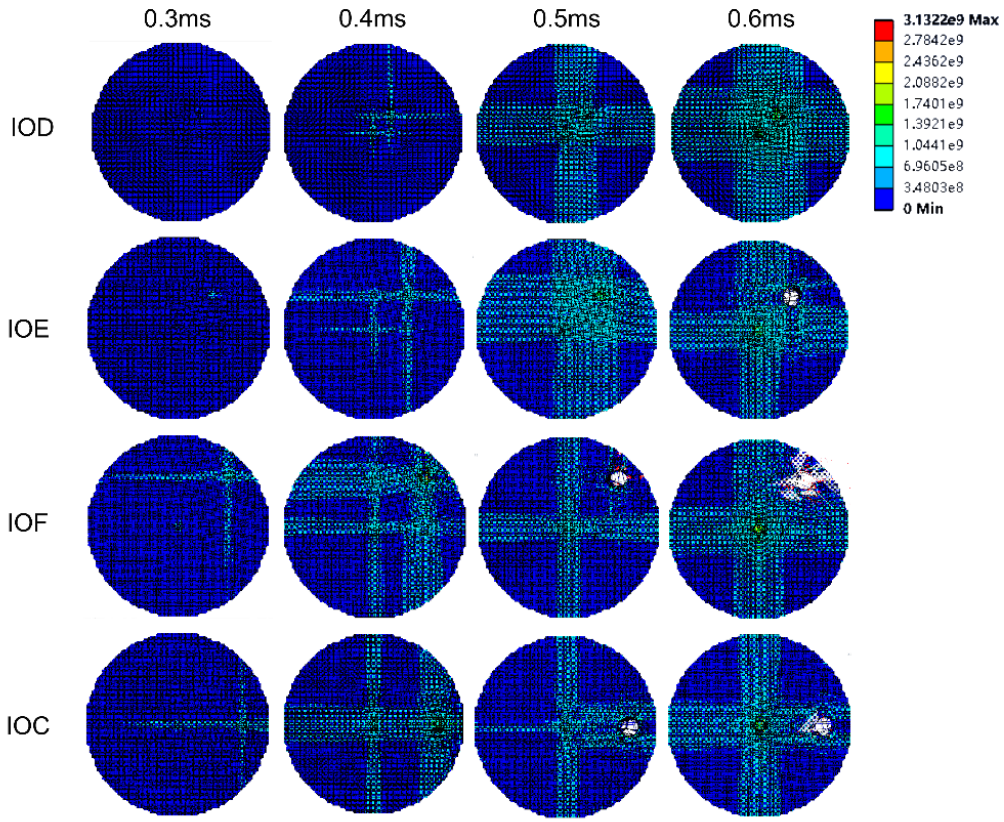


*Fig. 10. Comparison of fabric's stress distribution contours in asymmetrical impact scenarios*

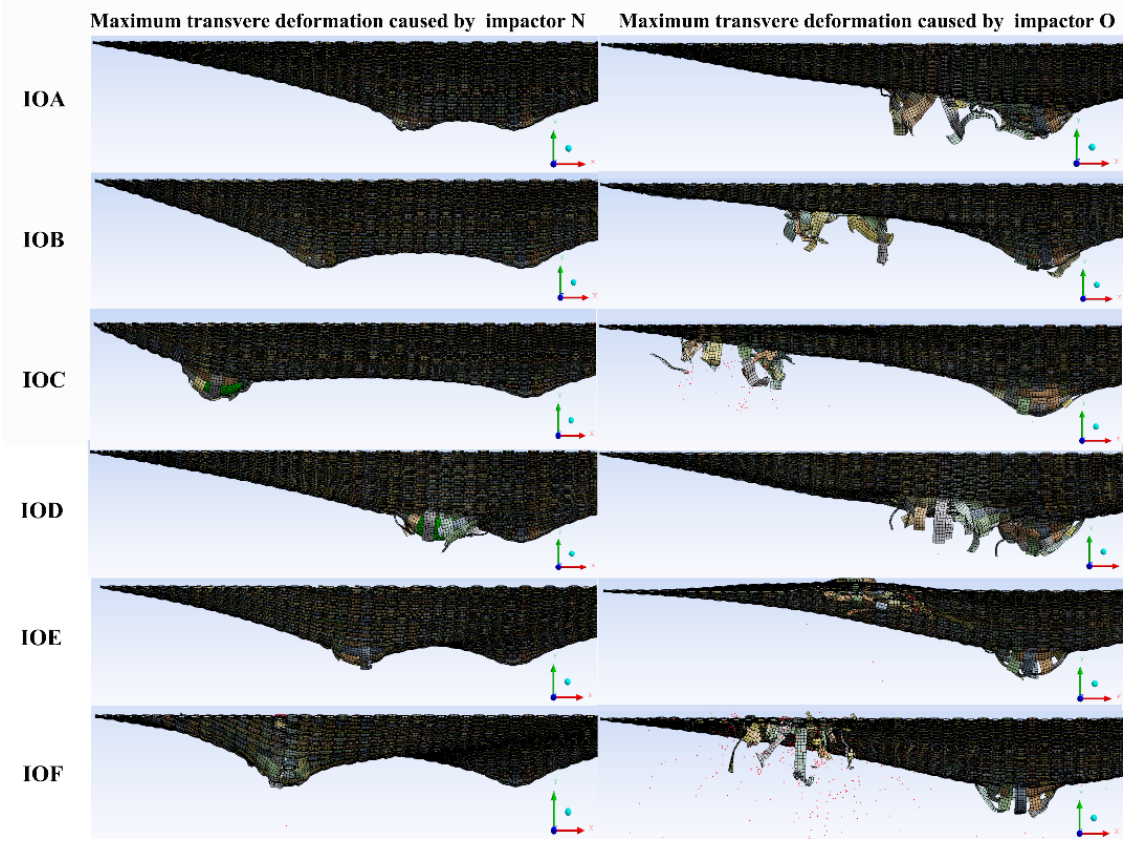


*Fig. 11. Comparison of fabric's transverse deformation in asymmetrical impact scenarios*

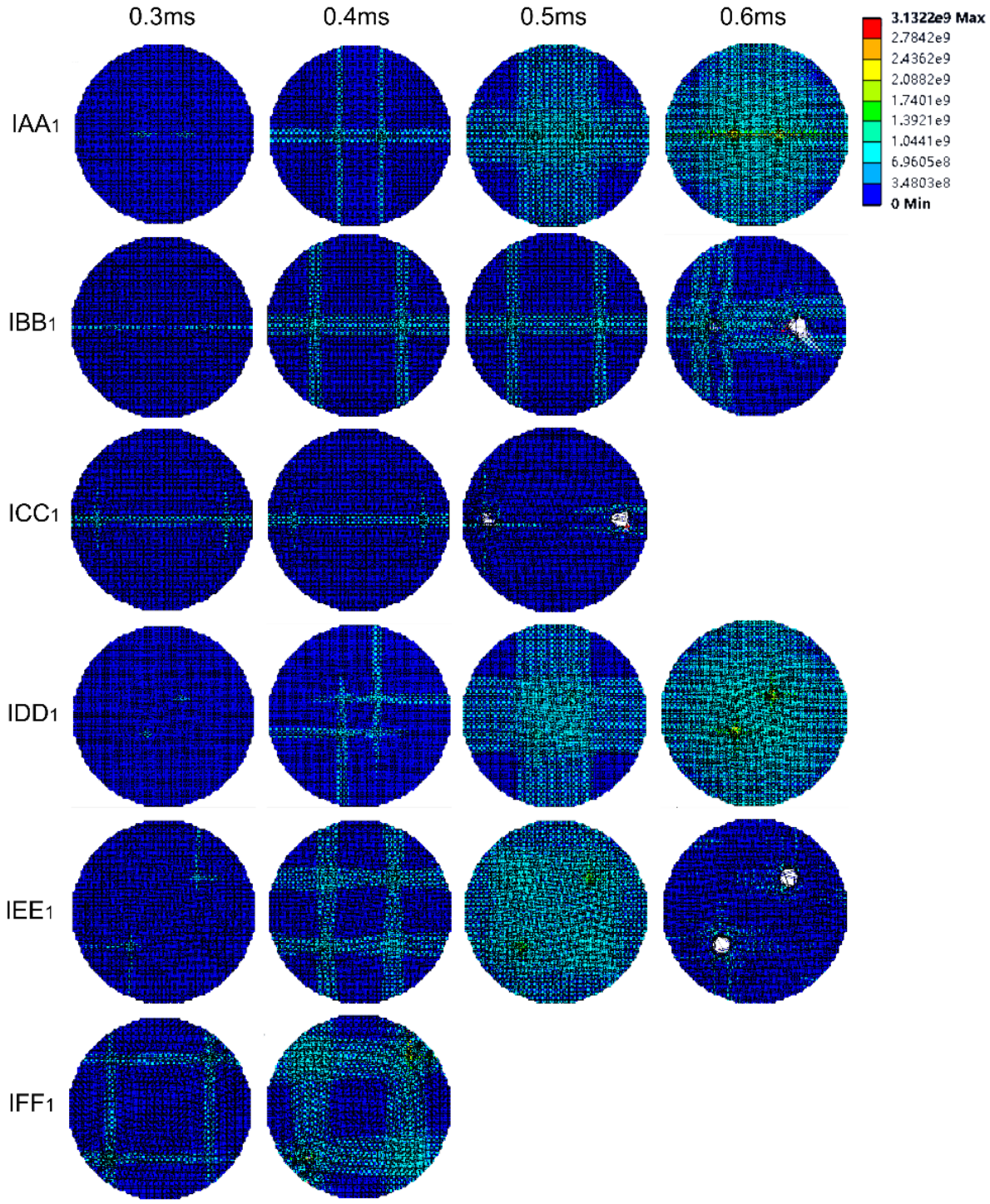


*Fig. 12. Comparison of fabric stress distribution contours in symmetrical impact scenarios*

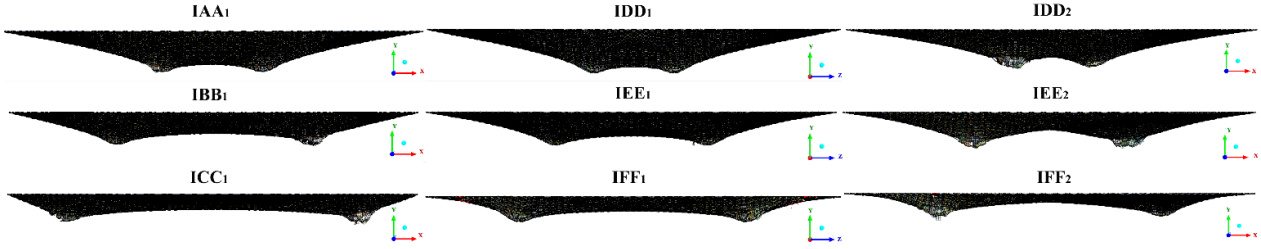


*Fig. 13. Comparison of fabric transverse deformation in symmetrical impact scenarios*

| $V_1$(m/s) | $V_2$ (m/s) | $MF_1$ (N) | $MF_2$(N) | $T_1$ (ms) | $T_2$ (ms) | ET (J) |
|---|---|---|---|---|---|---|
| 10 | 10 | 753.6 | 753.6 | 0.684 | 0.684 | 2.20 |
| 10 | 9 | 761.3 | 687.4 | 0.692 | 0.721 | 2.04 |
| 10 | 8 | 766.6 | 566.9 | 0.696 | 0.743 | 1.92 |
| 10 | 7 | 769.8 | 552.3 | 0.699 | 0.776 | 1.66 |

*Table 1. Impact results of the effect of velocity on the fabric's impact behaviors in scenario $IDD_1$*

| $V_O$ (m/s) | $V_C$ (m/s) | $MF_O$ (N) | $MF_C$ (N) | $T_O$ (ms) | $T_C$ (ms) | ET (J) |
|---|---|---|---|---|---|---|
| 10 | 10 | 467.3 | 559.5 | 0.580 | 0.468 | 1.62 |
| 10 | 9 | 496.1 | 546.4 | 0.603 | 0.512 | 1.59 |
| 10 | 8 | 519.4 | 510.8 | 0.626 | 0.554 | 1.46 |
| 10 | 7 | 553.9 | 481.2 | 0.642 | 0.607 | 1.38 |
| 9 | 10 | 458.8 | 559.3 | 0.712 | 0.474 | 1.54 |
| 8 | 10 | 452.1 | 561.6 | 0.806 | 0.478 | 1.46 |
| 7 | 10 | 446.4 | 560.3 | 0.938 | 0.466 | 1.40 |

*Table 2. Impact results of the effect of velocity on the fabric's impact behaviors in scenario IOC*

shorter the average distance between the impact location of the two impactors from the fixed boundary, the smaller the overall average failure deflection occurs.

– Among all asymmetrical impact scenarios, the fabric performed best regarding total energy absorption in scenario IOD with 1.93J, while the poorest performance appeared in scenario IBC - 1.34J. The total energy absorption in scenario $IDD_1$ is 2.20J, which performed best among all asymmetrical and symmetrical scenarios, while the poorest performance appears in scenario IBC with 1.26J, which is also the poorest performance among all asymmetrical and symmetrical scenarios.
– Variation in the Von-Mises stress distribution contours showed in the asymmetrical impact scenarios with one impactor impact at the fabric center, resulting in larger maximum stress and a wider stressed area under the same impact moment as impactor N moved farther from the center of the fabric. Fabrics under impactor O are always harder to puncture than under impactor N. The maximum transverse deformation caused by impactors becomes smaller as the impact point moves further away from the center of the fabric in both asymmetrical and symmetrical scenarios.
– Under both symmetrical and asymmetrical impact scenarios, when the impact energy is enough to puncture the fabric, the lower the average impact velocity of impactors, the weaker the energy absorption capacity of the fabric.

## Acknowledgements

The authors gratefully acknowledge the financial support from the Fujian Provincial Department of Science and Technology, for the Project of Natural Science Foundation of Fujian Province (No. 2022J011111) an the Guiding Project (No.2022H0048). We also gratefully acknowledge the financial support from Quanzhou Dongnuo Technology Co., Ltd for Project 2021K20.

## References


1. Nilakantan, Gaurav, and Steven Nutt. Effects of ply orientation and material on the ballistic impact behavior of multilayer plain-weave aramid fabric targets. Defence technology 14.3 (2018): 165-178.
2. Yang, Cheng-Chou, Tuan Ngo, and Phuong Tran. Influences of weaving architectures on the impact resistance of multi-layer fabrics. Materials & Design 85 (2015): 282-295.
3. Nipanjan Nayak, Chandra Sekher, Yerramalli, AsimTewari. Experimental investigation of the impact resistance on KEVLAR XP S308® fabric impacted with truncated ogive projectile subjected to pre-tension. Int J Impact Eng 2022,163, 104165.
4. Hongxu Wang, DakshithaWeerasinghe, DamithMohotti, Paul J.Hazell, V.P.W.Shim, KrishnaShankar, Evgeny V. Morozov. On the impact response of UHMWPE woven fabrics: Experiments and simulations. International Journal of Mechanical Sciences. 2021,204, 106574.
5. Yanfei Yang, Yanchen Liu, Sainan Xue, Xiangling Sun. Multi-scale finite element modeling of ballistic impact onto woven fabric involving fiber bundles. Composite Structures,2021,267, 113856.
6. Haolei Mou, Jiang Xie, Hui Pei, Zhenyu Feng, Hongzhang Geng. Ballistic impact tests and stacked shell simulation analysis of aramid fabric containment system. Aerospace Science and Technology. 2020, 107, 106344.
7. Xu, Wanli, Zhijia Dong, and Pibo Ma. Finite element analyses of auxetic warp-knitted fabric deformation behaviors under low-velocity impact loading. The Journal of The Textile Institute 111.11 (2020): 1578-1586.
8. Zeng, Haoxian, Xiaogang Chen, and Yanfei Yang. Influences of Combined Section in Three-dimensional Networked Fabric against Ballistic Impact. Applied Composite Materials (2021): 1-15.
9. Palta Emre, Fang Howie. On a multi-scale finite element model for evaluating ballistic performance of multi-ply woven fabrics. Composite Structures 2019; 207:488–580.
10. Giannaros, E, Kotzakolios, A., Sotiriadis, G., Tsantzalis, S, & Kostopoulos, V. On fabric materials response subjected to ballistic impact using meso-scale modeling. Numerical simulation and experimental validation. Composite Structures, 204(2018), 745-754.
11. Yang, Yanfei, and Xiaogang Chen. Influence of fabric architecture on energy absorption efficiency of soft armour panel under ballistic impact. Composite Structures 224 (2019): 111015.
12. Chu, Y, Rahman, M. R, Min, S., & Chen, X. Experimental and numerical study of inter-yarn friction affecting mechanism on ballistic performance of Twaron® fabric. Mechanics of Materials, 148(2020), 103421.
13. Miao, H., Wu, Z., Ying, Z., & Hu, X.. The numerical and experimental investigation on low-velocity impact response of composite panels: Effect of fabric architecture. Composite Structures, 227(2019), 111343.
14. Yadav, K., Upadhyay, A. K., & Shukla, K. K. Effect of obliquity on ballistic impact response of plain-woven fabric. International Journal of Materials and Structural Integrity, (2019)13(1-3), 93-109.
15. Feito, N., Loya, J. A., Muñoz-Sánchez, A., & Das, R. Numerical modelling of ballistic impact response at low velocity in aramid fabrics. Materials, (2019)12(13), 2087.
16. Palta, Emre, and Howie Fang. On a multi-scale finite element model for evaluating ballistic performance of multi-ply woven fabrics.Composite Structures 207 (2019): 488-508.
17. Grujicic M, Hariharan a, Pandurangan B, Yen CF, Cheeseman Ba, Wang Y, Zheng JQ. Fiber-level modeling of dynamic strength of kevlar® KM2 ballistic fabric. J Mater Eng Perform 2012;21(7):1107–19.
18. Zhang, Y, Ju, J. W, Zhu, H, Guo, Q, & Yan, Z. Micromechanics based multi-level model for predicting the coefficients of thermal expansion of hybrid fiber reinforced concrete. Construction and Building Materials, 190(2018), 948-963.
19. Ivanov I, Tabiei A. Loosely woven fabric model with viscoelastic crimped fibers for ballistic impact simulations. Int J Numer Meth Eng 2004;61(10):1565–83.
20. Shahkarami a, Vaziri R. A continuum shell finite element model for impact simulation of woven fabrics. Int J Impact Eng 2007;34(1):104–19.
21. Fang H, Gutowski M, Disogra M, Wang Q. A numerical and experimental study of woven fabric material under ballistic impacts. Adv Eng Softw (2016), 96:14–28.
22. Liu, L, Yang, Z., Liu, X, Chen, W, Zhao, Z, & Luo, G. Yarn dynamic tensile behavior and meso-scale numerical simulation method for STF-Kevlar fabrics. Thin-Walled Structures, 159 (2021), 107319.
23. Zeng, H., Chen, X., & Yang, Y.. Influences of Combined Section in Three-dimensional Networked Fabric against Ballistic Impact. Applied Composite Materials, (2021)1-15.
24. Giannaros, E., Kotzakolios, A., Sotiriadis, G., Tsantzalis, S., & Kostopoulos, V. On fabric materials response subjected to ballistic impact using meso-scale modeling. Numerical simulation and experimental validation. Composite Structures, 204, (2018) 745-754.
25. Priyanka, P, Mali, H. S, & Dixit, A. Mesoscale numerical characterization of Kevlar and carbon–Kevlar hybrid plain-woven fabric compression behavior. Journal of Materials Engineering and Performance, (2019)28(9), 5749-5762.
26. Feito, N., Loya, J. A., Muñoz-Sánchez, A., & Das, R. Numerical modelling of ballistic impact response at low velocity in aramid fabrics. Materials, (2019)12(13), 2087.
27. Canyi Huang, Lina Cui, Hong Xia, Yiping Qiu, Qing-Qing Ni. A numerical study on the influence of hole defects on impact behavior of Twaron® fabric subjected to low-velocity impacts. Journal of Engineered Fibers and Fabrics, 2021,16: 1–18.
28. Wang, H, Weerasinghe, D, Mohotti, D, Hazell, P. J, Shim, V. P. W, Shankar, K., & Morozov, E. V. On the Impact Response of UHMWPE Woven Fabrics: Experiments and Simulations. International Journal of Mechanical Sciences, (2021)106574.
29. Canyi Huang, Lina Cui, Yajun Liu, Hong Xia, Yiping Qiu, Qing-Qing Ni. Low-velocity drop weight impact behavior of Twaron® fabric investigated using experimental and numerical simulations. Int J Impact Eng, (2021)149, 103796.

30. Canyi Huang, Lina Cui, Hong Xia, Yiping Qiu, Qing-Qing Ni. A numerical study on the low-velocity impact behavior of the Twaron® fabric subjected to oblique impact. Reviews on Advanced Materials Science, 2021,60:980-994.
31. Hairong Miao, Zhenyu Wu, Zhiping Ying, Xudong Hu. The numerical and experimental investigation on low-velocity impact response of composite panels: Effect of fabric architecture. Composite Structures 227 (2019) 111343.
32. Canyi Huang, Lina Cui, Hong Xia, Yiping Qiu, Qing-Qing Ni. Influence of crimp and inter-yarn friction on the mechanical properties of woven fabric under uniaxial/ biaxial tensile loading. FIBRES & TEXTILES in Eastern Europe, 2020(28): 43-52.
33. Yanfei Yang, Xiaogang Chen. Investigation on energy absorption efficiency of each layer in ballistic amour panel for applications in hybrid design. Composite Structure, 164 (2017), pp. 1-9.